Staggered Vertical Discretization of the Canadian Environmental Multiscale (GEM) Model Using a Coordinate of the Log-Hydrostatic-Pressure Type

CLAUDE GIRARD

Recherche en Prévision Numérique Atmosphérique, Environment Canada, Dorval, Quebec, Canada

ANDRÉ PLANTE

Canadian Meteorological Centre, Environment Canada, Dorval, Quebec, Canada

MICHEL DESGAGNÉ, RON MCTAGGART-COWAN, JEAN CÔTÉ, MARTIN CHARRON, SYLVIE GRAVEL, VIVIAN LEE, ALAIN PATOINE, ABDESSAMAD QADDOURI, MICHEL ROCH, LUBOS SPACEK, MONIQUE TANGUAY, PAUL A. VAILLANCOURT, AND AYRTON ZADRA

Recherche en Prévision Numérique Atmosphérique, Environment Canada, Dorval, Quebec, Canada

(Manuscript received 13 August 2013, in final form 23 October 2013)

ABSTRACT

The Global Environmental Multiscale (GEM) model is the Canadian atmospheric model used for meteorological forecasting at all scales. A limited-area version now also exists. It is a gridpoint model with an implicit semi-Lagrangian iterative space–time integration scheme. In the ''horizontal,'' the equations are written in spherical coordinates with the traditional shallow atmosphere approximations and are discretized on an Arakawa C grid. In the ''vertical,'' the equations were originally defined using a hydrostatic-pressure coordinate and discretized on a regular (unstaggered) grid, a configuration found to be particularly susceptible to noise. Among the possible alternatives, the Charney–Phillips grid, with its unique characteristics, and, as the vertical coordinate, log-hydrostatic pressure are adopted. In this paper, an attempt is made to justify these two choices on theoretical grounds. The resulting equations and their vertical discretization are described and the solution method of what is forming the new dynamical core of GEM is presented, focusing on these two aspects.

1. Introduction

An integrated forecasting and data assimilation system is under continual development at Recherche en Prévision Numérique Atmosphérique (RPN) in partnership with the Canadian Meteorological Centre (CMC) of Environment Canada. The initial basic hydrostatic formulation of the CMC-RPN Global Environmental Multiscale (GEM) model used in the forecasting system is described by Côté et al. (1998). A nonhydrostatic extension using the hydrostatic pressure coordinate of Laprise (1992) is given by Yeh et al. (2002). Originally designed to operate solely in the global mode while using variable resolution for regional modeling applications, the model (GEM3) is now equipped with a limited-area model (LAM) configuration due to a technology transfer from the Mesoscale Compressible Community (MC2) model (Thomas et al. 1998). Presently, the option of making global integrations on a dual-LAM Yin–Yang grid is being developed (Qaddouri and Lee 2011).

Perhaps the most characteristic feature of the model is its implicit semi-Lagrangian iterative space–time integration scheme. Due to the fourth-order accuracy of its treatment of nonlinear advection, finite differences are found to provide sufficient accuracy for the spatial discretization of the remaining terms. This in fact constitutes a radical change of paradigm for CMC-RPN from the previous forecasting system. In effect, GEM3 has replaced, for global integrations, a spectral model with finite elements in the vertical (Ritchie 1991) and, for regional integrations, a model with finite elements in the horizontal and finite differences in the vertical

Corresponding author address: Claude Girard, 2121 TransCanada Highway, Ste. 500, Dorval, QC H9P 1J3, Canada.
E-mail: claude.girard@ec.gc.ca

DOI: 10.1175/MWR-D-13-00255.1

(Tanguay et al. 1989). Both models were defined on regular[1] (unstaggered) grids in the horizontal as well as in the vertical. On the other hand, the finite-difference horizontal discretization of GEM3 employs the Arakawa C grid (Arakawa 1988) in spite of the added complexity for the semi-Lagrangian treatment of horizontal wind components (Côté et al. 1998). In the vertical, the grid remains regular (R grid).

Noise problems were diagnosed in GEM3, related to vertical discretization on the R grid. In particular, the presence of numerical ($2\,\Delta z$) modes was clearly detected by singular vector analysis (Zadra et al. 2004). Similar, though less serious, problems with stationary computational modes have been diagnosed by Arakawa and Moorthi (1988), Hollingsworth (1995), and Arakawa and Konor (1996) on the Lorenz (1960) (L) grid and simultaneously shown to be absent on the Charney and Phillips (1953) (CP) grid. The findings of Zadra et al. (2004), along with a model behavior in terms of noise very much resembling the ones documented in the above-mentioned studies, prompted us to reexamine the issue of vertical discretization in GEM3, particularly since it seemed to be the only operational NWP model using the R grid. While advocating for the CP grid, Arakawa and Konor (1996) noted that it was ''not widely used in the primitive equation models because it is easier with the L grid to maintain some of the integral properties of the continuous system''. Nevertheless, there are a few studies that demonstrate the utility (Robert et al. 1972, Yakimiw and Girard 1987, Tanguay et al. 1990, Girard et al. 2005) as well as the potential for conservation (Laprise and Girard 1990, Arakawa and Konor 1996) of the CP grid.

The grid issue is usually considered to be one of positioning of the discrete variables and its impacts on computational stability and accuracy. Computational dispersion properties of the linear equations are also an important consideration. In the vertical, with four variables and two positions, eight different grid-variable configurations may be constructed (Tokioka 1978). In reality, the grid issue is more complex since, as will be shown, with four quite simple equations in four variables on two positions, up to 41 grid-equation-variable configurations are possible and indeed more configurations can be considered if we add the time dimension (Fox-Rabinovitz 1994). Surprisingly, the R grid as defined and used in GEM3 has not been previously discussed even though it is comparable to the CP and L grids in terms of stability, accuracy, and dispersion properties.

[1] Here, we use the term ''regular,'' following Fox-Rabinovitz (1994), to describe a grid system in which all variables are collocated.

Even once a grid is decided upon, there remains flexibility in the choice of coordinate and history-carrying variables within the context of the Euler equations (Thuburn and Woollings 2005). A height-based coordinate, for example, is certainly a valid option. An incremental approach to development suggested, however, a straightforward introduction of staggering (the strict conversion from the R to the CP grid) as a first step. Many arguments, though, played in favor of at least a ''mild'' change of coordinate, from the original terrain following of hydrostatic-pressure type (Yeh et al. 2002) of GEM3 to one of log-hydrostatic-pressure type for GEM4 (this presently described version of GEM), which we are calling the ζ coordinate.

The grid issue is addressed in section 2 with emphasis on the unique properties of the CP grid. The derivation of the Euler equations in the ζ coordinate is made in section 3. They are vertically discretized on the CP grid in section 4. In section 5, the main elements of the solution method are presented and we end with a summary in section 6.

2. Unique properties of the Charney–Phillips grid

a. Equations: Full and linearized

The dynamical equations of GEM originate from the standard Euler set of meteorological equations:

$$\frac{d\mathbf{V}}{dt} + f\mathbf{k}\times\boldsymbol{V} + \frac{1}{\rho}\nabla p + g\mathbf{k} = \mathbf{F}, \tag{1}$$

$$\frac{dT}{dt} - \frac{1}{\rho c_p}\frac{dp}{dt} = \frac{Q}{c_p}, \tag{2}$$

$$\frac{d\ln\rho}{dt} + \nabla\cdot\mathbf{V} = 0, \quad \text{and} \tag{3}$$

$$\rho = \frac{p}{RT}. \tag{4}$$

For the present purpose, the ''horizontal'' not being a concern, we choose a Cartesian coordinate system as our initial model framework. The four independent $[t, \mathbf{r} = (\mathbf{r}_h, z) = (x, y, z)]$ and six dependent $[\mathbf{V} = (\mathbf{V}_h, w) = (u, v, w)$, T, p, $\rho]$ variables, as well as all other symbols, will have their usual meaning. There are five prognostic equations [momentum, (1); energy, (2); and mass conservation, (3)] and the ideal gas law [(4)]. The Coriolis force is given its traditional approximated form. The shallow atmosphere approximation (Phillips 1966) is kept in GEM4. Minimally, this system of equations needs to be augmented and modified to take into account moisture effects. For the present purpose though, the strictly

dynamical system suffices. For the same reason, friction **F** and heat sources Q will be set to vanish and the thermodynamic parameters R and c_p will be treated as constants.

Immediately, we would like to comment on the discretization of diagnostic relations. Analytically, a variable defined through a diagnostic relation can always be eliminated. If such elimination is done prior to discretization, approximations may be avoided, especially when the variables are not collocated. In meteorological applications this is frequently the case for density. Doing so yields a set of five equations in five unknowns:

$$\frac{d\mathbf{V}}{dt} + f\mathbf{k}\times\mathbf{V} + RT\nabla \ln p + g\mathbf{k} = 0, \tag{5}$$

$$\frac{d\ln T}{dt} - \kappa\frac{d\ln p}{dt} = 0, \quad \text{and} \tag{6}$$

$$(1-\kappa)\frac{d\ln p}{dt} + \nabla\cdot\mathbf{V} = 0, \tag{7}$$

where $\kappa = R/c_p$. Note that $\ln p$ may be viewed in two different ways: as a completely independent variable or as a numerical operation on the original variable p. Such an operation will tend to interfere with other numerical operations such as averaging ($\overline{\ln p}$ versus $\ln\overline{p}$) or differencing ($\Delta\ln p$ versus $\Delta p/p$). In fact, having $\ln p$ as a new variable is a serious option here since p no longer occurs by itself. Let us linearize the above equations around an isothermal basic state at rest, neglecting the Coriolis force. Keeping a single dimension in the horizontal, we obtain

$$\partial_t u + \partial_x P = 0, \tag{8}$$

$$\partial_t w + \partial_z P - b = 0, \tag{9}$$

$$\partial_t b - g\partial_t P/c_P T_* + N_*^2 w = 0, \quad \text{and} \tag{10}$$

$$\partial_t P/c_*^2 + \partial_x u + \partial_z w - gw/c_*^2 = 0, \tag{11}$$

with the notation $\partial_\lambda \equiv \partial/\partial\lambda$. The four dependent variables are the wind components, u and w; the pressure-related $P = RT_*(\ln p)'$; and the buoyancy-related $b = gT'/T_*$. There are two characteristic parameters: the Brunt–Vaïsälä frequency, $N_* = \sqrt{g^2/c_p T_*}$, and the speed of sound, $c_* = \sqrt{RT_*/(1-\kappa)}$.

b. Vertical structures: Analytic and discrete

A set of standard approximations allow us to simplify this set of linear equations. The second term in (10) and the last term in (11) represent the pressure contribution to buoyancy and the effect of stratification on compressibility, respectively. In the following discussion, we exclude them by adopting the Boussinesq approximation for a thin fluid, a fairly common procedure in such analyses. As will become evident in the discussion, they are terms requiring averaging on the CP grid: the only ones in fact. This property is unique to the CP grid. We also neglect for simplicity the vertical wind tendency (hydrostatic assumption) and the pressure tendency (incompressibility assumption), even though not requiring averaging on the CP grid. Considering typical eigensolutions $e^{i(kx+\nu t)}$ and replacing the time and horizontal differential operators by their eigenvalues, (8)–(11) become

$$i\nu u + ikP = 0,$$

$$\partial_z P - b = 0,$$

$$i\nu b + N_*^2 w = 0, \quad \text{and}$$

$$iku + \partial_z w = 0.$$

We thus obtain the analytic vertical structure equation:

$$(\partial_z^2 + n^2)P = 0,$$

with $n = \pm kN_*/\nu$ and with vertical analytic eigensolutions $E = e^{inz}$. We adopt the standard second-order-accurate central differencing, for which the basic difference (δ_z) and averaging (μ_z or denoted by an overbar) operators are

$$\delta_z E = \frac{E(z+\Delta z/2) - E(z-\Delta z/2)}{\Delta z} = \rho_-\partial_z E \quad \text{and}$$

$$\overline{E} = \mu_z E = \frac{E(z+\Delta z/2) + E(z-\Delta z/2)}{2} = \rho_+ E,$$

with the response functions given by

$$\rho_- = \frac{\sin(n\Delta z/2)}{n\Delta z/2} \quad \text{and}$$

$$\rho_+ = \cos(n\Delta z/2).$$

Table 1 lists the 12 semidiscrete equations that can thus be formed, three sets of four, labeled according to averaging requirements: x if no averaging is needed, a if averaging is needed and applied on the first term, and b if averaging is needed but applied on the second term. Table 2 lists the eight possible grids. Table 3 lists all of the 41 possible grid-equation configurations (i.e., combinations of equations that can be formed) along with the resulting discrete vertical structure equations. Note that, unlike the unique analytic equation, there

TABLE 1. Twelve semidiscrete structure equations, classified according to their vertical averaging requirements: no averaging x, first term averaging a, and second term averaging b.

	x	a	b
1	$i\nu u + ikP = 0$	$i\nu\overline{u} + ikP = 0$	$i\nu u + ik\overline{P} = 0$
2	$\delta_z w + iku = 0$	$\delta_z\overline{w} + iku = 0$	$\delta_z w + ik\overline{u} = 0$
3	$\delta_z P - b = 0$	$\delta_z\overline{P} - b = 0$	$\delta_z P - \overline{b} = 0$
4	$i\nu b + N_*^2 w = 0$	$i\nu\overline{b} + N_*^2 w = 0$	$i\nu b + N_*^2\overline{w} = 0$

TABLE 2. Eight discretization strategies for positioning four variables in two grid positions and associated grid numbers (g1–g8).

g1	———	u, P	g5	———	u
	– – – – –	w, b		– – – – –	P, w, b
g2	———	u, P, w, b	g6	———	u, w, b
	– – – – –			– – – – –	P
g3	———	u, P, b	g7	———	u, P, w
	– – – – –	w		– – – – –	b
g4	———	u, b	g8	———	u, w
	– – – – –	w, P		– – – – –	P, b

may be up to four discrete equations per configurations differing by one or even two averaging operators, depending on the variable, u, w, P, or b, chosen in the elimination process.

Looking at Table 3 heuristically, the presence of an averaging operator must be seen as reducing accuracy as well as potentially providing support for computational modes. We highlight four main configurations: CP, R, and a pair of L-type grids, L^a and L^b. We also identify the eight configurations as analyzed by Tokioka (1978): A, B, C, D, A′, B′, C′, and D′. Grid g1, the CP grid, admits a single configuration, additional evidence of its unique properties. Grids g2–g7 each allow four types of configurations. The first type, with two equations taken from set a, simply leads to inaccurate systems since derivatives are evaluated over two grid lengths instead of a single one. Fox-Rabinovitz (1994) chose g2 ($1x$, $2a$, $3a$, $4x$) as his regular grid configuration, which is characterized by the absence of staggering in both variables and equations. The second and third types, with one equation taken from set a, suffer from special computational solutions resulting from the presence of an additional averaging operator appearing on some of the discrete structure equations. Tokioka (1978) demonstrated the presence of such modes ($n\Delta z = \pm\pi$) for vertical motion w in four of his schemes, in particular his choice of regular grid, configuration g2 ($1x$, $2a$, $3b$, $4x$), his scheme D. Configurations of the fourth type, with no equation taken from set a, all result in the same and unique discrete vertical structure equation; hence, there is no computational solution of the type mentioned above. We find in this type the other three grid-equation configurations of interest: the R [g2 ($1x$, $2b$, $3b$, $4x$)], L^a [g3 ($1x$, $2x$, $3b$, $4b$)], and L^b [g4 ($1b$, $2x$, $3x$, $4b$)] configurations. For completeness, we list all 16 configurations of grid g8: none are able to compete with any of the previous examples since they either are less accurate or suffer from additional computational modes.

c. *Configurations CP, R, L^a, and L^b: Their properties*

Restricting our attention to these four configurations, only two discrete vertical structure equations are involved. The first one corresponds to the CP configuration, the second to the others. Horizontal and vertical phase speeds (c_x and c_z), as well as group velocities ($c_{g,x}$ and $c_{g,z}$), have often been compared between the CP and L grids. Here, the results are summarized in Tables 4 and 5, respectively. We emphasize the fact that configuration R has the same basic dispersive properties as the L configurations, according to the limited analysis framework adopted here (pure gravity wave modes). The maximum wavenumber in the vertical is given by $n_{\max} = 2\pi/\lambda_{\min}$ ($\lambda_{\min} = 2\Delta z$). In the horizontal, phase speeds and group velocities are identically defined analytically. Numerically, they are overestimated with the CP configuration, underestimated with the others. The CP configuration is slightly more accurate. In the vertical, analytic phase speeds and group velocities have the same amplitude but opposite sign. Numerically, amplitude differs but signs remain correct, an important feature for group velocities. Ratios of numerical to analytical phase speeds and vertical group velocities for the CP (thick solid lines) and the other three configurations (dashed lines) are depicted in Figs. 1 and 2, respectively. Fundamentally, though, the four configurations may be said to be fairly equivalent in these respects.

In Table 6 the numerical schemes and corresponding computational grids for these four configurations are explicitly shown. It is not possible to have all dependent variables collocated in the L configurations. This is a property of g2 configurations (Table 3), of which R (GEM3) is a member. The g2 configurations only differ by staggering of the equations. In this case, R is characterized by staggering of the vertical momentum (hydrostatic) and continuity (divergence) equations with respect to the horizontal momentum and thermodynamic equations, staggering necessary to achieve second-order accuracy. Note the complete absence of staggering of equations in L^b, a property that facilitates the development of conservative schemes.

There is yet another very important difference between these four configurations, namely the absence or presence of stationary numerical modes ($\nu = 0$). Such modes also occur in the presence of averaging operators.

TABLE 3. Forty-one [1 + 6 × 4 + 16] resulting grid-equation configurations, i.e., ways to discretize four equations (Table 1) involving four variables and their two grid positions (Table 2). In the first column are the grid numbers, in the second the configuration identifier, in the third the names given to the four main configurations discussed in the text, in the fourth column the names originally given by Tokioka (1978) to eight configurations, and in the last column the corresponding numerical structure equations.

g1	$\{1x, 2x, 3x, 4x$	CP	B	$(\delta_{zz} + n^2)[u, w, P, b] = 0$
g2	$1x, 2a, 3a, 4x$			$(\mu_{zz}\delta_{zz} + n^2)[u, w, P, b] = 0$
	$1x, 2a, 3b, 4x$		D	$(\delta_{zz} + n^2)[u, \overline{w}, P, \overline{b}] = 0$
	$1x, 2b, 3a, 4x$			$(\delta_{zz} + n^2)[\overline{u}, w, \overline{P}, b] = 0$
	$1x, 2b, 3b, 4x$	R		$(\delta_{zz} + n^2\mu_{zz})[u, w, P, b] = 0$
g3	$1x, 2x, 3a, 4a$			$(\mu_{zz}\delta_{zz} + n^2)[u, w, P, b] = 0$
	$1x, 2x, 3a, 4b$			$(\delta_{zz} + n^2)[\overline{u}, \overline{w}, \overline{P}, b] = 0$
	$1x, 2x, 3b, 4a$			$(\delta_{zz} + n^2)[u, w, P, \overline{b}] = 0$
	$1x, 2x, 3b, 4b$	L^a	A	$(\delta_{zz} + n^2\mu_{zz})[u, w, P, b] = 0$
g4	$1a, 2x, 3x, 4a$			$(\mu_{zz}\delta_{zz} + n^2)[u, w, P, b] = 0$
	$1a, 2x, 3x, 4b$			$(\delta_{zz} + n^2)[\overline{u}, \overline{w}, P, b] = 0$
	$1b, 2x, 3x, 4a$			$(\delta_{zz} + n^2)[u, w, \overline{P}, \overline{b}] = 0$
	$1b, 2x, 3x, 4b$	L^b	C′	$(\delta_{zz} + n^2\mu_{zz})[u, w, P, b] = 0$
g5	$1a, 2x, 3a, 4x$			$(\mu_{zz}\delta_{zz} + n^2)[u, w, P, b] = 0$
	$1a, 2x, 3b, 4x$			$(\delta_{zz} + n^2)[\overline{u}, \overline{w}, P, \overline{b}] = 0$
	$1b, 2x, 3a, 4x$			$(\delta_{zz} + n^2)[u, w, \overline{P}, b] = 0$
	$1b, 2x, 3b, 4x$		D′	$(\delta_{zz} + n^2\mu_{zz})[u, w, P, b] = 0$
g6	$1a, 2a, 3x, 4x$			$(\mu_{zz}\delta_{zz} + n^2)[u, w, P, b] = 0$
	$1a, 2b, 3x, 4x$			$(\delta_{zz} + n^2)[\overline{u}, w, P, b] = 0$
	$1b, 2a, 3x, 4x$		B′	$(\delta_{zz} + n^2)[u, \overline{w}, \overline{P}, \overline{b}] = 0$
	$1b, 2b, 3x, 4x$			$(\delta_{zz} + n^2\mu_{zz})[u, w, P, b] = 0$
g7	$1x, 2a, 3x, 4a$			$(\mu_{zz}\delta_{zz} + n^2)[u, w, P, b] = 0$
	$1x, 2a, 3x, 4b$		C	$(\delta_{zz} + n^2)[u, \overline{w}, P, b] = 0$
	$1x, 2b, 3x, 4a$			$(\delta_{zz} + n^2)[\overline{u}, w, \overline{P}, \overline{b}] = 0$
	$1x, 2b, 3x, 4b$			$(\delta_{zz} + n^2\mu_{zz})[u, w, P, b] = 0$
g8	$1a, 2a, 3a, 4a$			$(\mu_{zzzz}\delta_{zz} + n^2)[u, w, P, b] = 0$
	$1a, 2b, 3a, 4a$			$(\mu_{zz}\delta_{zz} + n^2)[\overline{u}, w, P, b] = 0$
	$1a, 2a, 3a, 4b$			$(\mu_{zz}\delta_{zz} + n^2)[u, \overline{w}, P, b] = 0$
	$1a, 2a, 3b, 4a$			$(\mu_{zz}\delta_{zz} + n^2)[u, w, \overline{P}, b] = 0$
	$1b, 2a, 3a, 4a$			$(\mu_{zz}\delta_{zz} + n^2)[u, w, P, \overline{b}] = 0$
	$1a, 2b, 3a, 4b$			$(\delta_{zz} + n^2)[\overline{u}, \overline{w}, \overline{P}, b] = 0$
	$1a, 2a, 3b, 4a$			$(\delta_{zz} + n^2)[\overline{u}, \overline{w}, P, \overline{b}] = 0$
	$1a, 2b, 3b, 4a$			$(\delta_{zz} + n^2)[\overline{u}, w, \overline{P}, \overline{b}] = 0$
	$1b, 2a, 3a, 4b$			$(\delta_{zz} + n^2)[u, \overline{w}, \overline{P}, b] = 0$
	$1b, 2b, 3a, 4a$			$(\delta_{zz} + n^2)[\overline{u}, w, \overline{P}, \overline{b}] = 0$
	$1b, 2a, 3b, 4a$			$(\delta_{zz} + n^2)[u, \overline{w}, \overline{P}, \overline{b}] = 0$
	$1a, 2b, 3b, 4b$			$(\delta_{zz} + n^2\mu_{zz})[\overline{u}, w, P, b] = 0$
	$1b, 2a, 3b, 4b$	A'		$(\delta_{zz} + n^2\mu_{zz})[u, \overline{w}, P, b] = 0$
	$1b, 2b, 3a, 4b$			$(\delta_{zz} + n^2\mu_{zz})[u, w, \overline{P}, b] = 0$
	$1b, 2b, 3b, 4a$			$(\delta_{zz} + n^2\mu_{zz})[u, w, P, \overline{b}] = 0$
	$1b, 2b, 3b, 4b$			$(\delta_{zz} + n^2\mu_{zzzz})[u, w, P, b] = 0$

Setting $\nu = 0$ in the horizontal momentum equation ($k \neq 0$) implies either $\overline{P}^z = 0$ in L^b configuration or $P = 0$, and therefore $\overline{b}^z = 0$ in the thermodynamic equation in R and L^a configurations. A stationary $2\Delta z$ mode is thus present and not seen by the rest of the scheme in these three configurations. This is the infamous mode as discussed by Arakawa and Moorthi (1988) or Hollingsworth (1995). What was found during the present study is that the R configuration of GEM3 supports a second stationary $2\Delta z$ mode in the vertical. Setting $\nu = 0$ in the thermodynamic equation implies $w = 0$, leading to $\overline{u}^z = 0$. In this case, a stationary $2\Delta z$ mode in the continuity equation is not seen by the rest of the scheme. This may explain the relatively high noise level present in GEM3. The absence of such stationary numerical modes in the CP configuration is the principal motivation for changing the vertical configuration of the GEM model.

TABLE 4. Exact and approximate discrete phase speeds in the horizontal c_x and vertical c_z directions as functions of wavenumber n.

Phase speed	$c_x(n) = \frac{\nu(n)}{k}$	$c_x(n_{\max})$	$c_z(n) = \frac{\nu(n)}{n}$	$c_z(n_{\max})$
Exact	$\frac{N_*}{n}$	$\frac{N_*\Delta z}{\pi}$	$\frac{kN_*}{n^2}$	$\frac{kN_*\Delta z^2}{\pi^2}$
CP	$\frac{1}{\rho_-}\frac{N_*}{n}$	$\frac{N_*\Delta z}{2}$	$\frac{1}{\rho_-}\frac{kN_*}{n^2}$	$\frac{kN_*\Delta z^2}{2\pi}$
R, L^a, L^b	$\frac{\rho_+}{\rho_-}\frac{N_*}{n}$	0	$\frac{\rho_+}{\rho_-}\frac{kN_*}{n^2}$	0

3. Equations: Vertical coordinate and history-carrying variables

A coordinate transformation of the basic equations (5)–(7) will bring us to a generalized vertical coordinate η. Here, we use η in a general unspecified sense. To achieve this, we simply need to apply standard rules of substitution for the differential operators (Kasahara 1974):

$$\nabla_z \equiv \nabla_\eta - \nabla_\eta z \frac{\partial \eta}{\partial z}\frac{\partial}{\partial \eta},$$

$$\frac{\partial}{\partial z} \equiv \frac{\partial \eta}{\partial z}\frac{\partial}{\partial \eta},$$

obtaining for the momentum (5) and continuity (7) equations, respectively,

$$\frac{d\mathbf{V}_h}{dt} + f\mathbf{k}\times\mathbf{V}_h + RT\left(\nabla_\eta \ln p - \nabla_\eta z \frac{\partial \eta}{\partial z}\frac{\partial \ln p}{\partial \eta}\right) = 0, \quad (12)$$

$$\frac{dw}{dt} + RT\frac{\partial \eta}{\partial z}\frac{\partial \ln p}{\partial \eta} + g = 0, \quad \text{and} \quad (13)$$

TABLE 5. Exact and approximate discrete group velocities in the horizontal $c_{g,x}$ and vertical $c_{g,z}$ directions as functions of wavenumber n.

Group velocity	$c_{g,x}(n) = \frac{\partial \nu(n)}{\partial k}$	$c_{g,x}(n_{\max})$	$c_{g,z}(n) = \frac{\partial \nu(n)}{\partial n}$	$c_{g,z}(n_{\max})$
Exact	$\frac{N_*}{n}$	$\frac{N_*\Delta z}{\pi}$	$-\frac{kN_*}{n^2}$	$-\frac{kN_*\Delta z^2}{\pi^2}$
CP	$\frac{1}{\rho_-}\frac{N_*}{n}$	$\frac{N_*\Delta z}{2}$	$-\frac{\rho_+}{\rho_-^2}\frac{kN_*}{n^2}$	0
R, L^a, L^b	$\frac{\rho_+}{\rho_-}\frac{N_*}{n}$	0	$-\frac{1}{\rho_-^2}\frac{kN_*}{n^2}$	$-\frac{kN_*\Delta z^2}{4}$

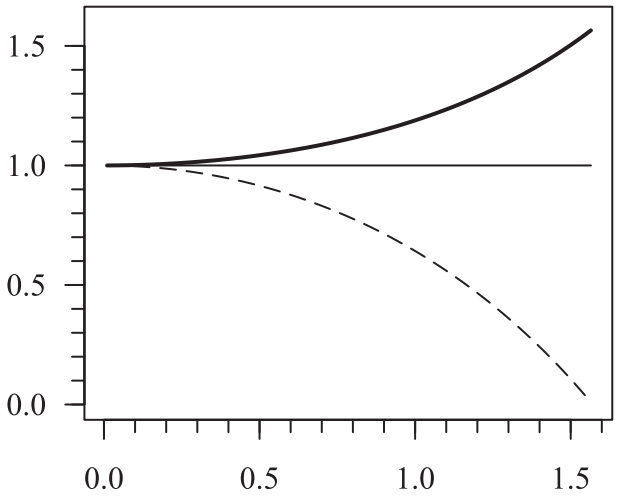

FIG. 1. Ratio to exact wave speed as a function of wavenumber n and vertical grid length Δz: CP grid (thick solid line), exact (thin solid line), and R and L grids (dashed line).

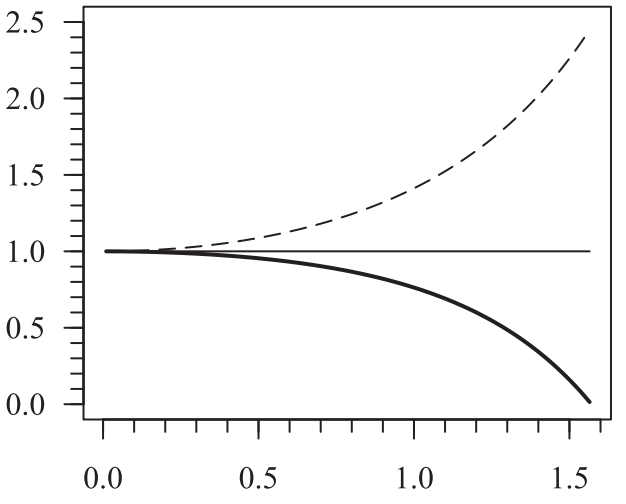

FIG. 2. Ratio to exact vertical group velocity as a function of wavenumber n and vertical grid length Δz: CP grid (thick solid line), exact solution (thin solid line), and R and L grids (dashed line).

$$\frac{d}{dt}\ln\left|\frac{p}{T}\frac{\partial z}{\partial \eta}\right| + \nabla_\eta \cdot \mathbf{V}_h + \frac{\partial \dot{\eta}}{\partial \eta} = 0. \tag{14}$$

We had to decompose the vector equation (5) into its horizontal [(12)] and vertical [(13)] components due to the different transformation rules. The transformation does not alter the form of the total derivative, which now reads

$$\frac{d}{dt} \equiv \frac{\partial}{\partial t} + \mathbf{V}_h \cdot \nabla + \dot{\eta}\frac{\partial}{\partial \eta}, \tag{15}$$

where $\dot{\eta} = d\eta/dt$. Consequently, the thermodynamic equation (6) is invariant. The transformation remains incomplete, though, and we are left with two vertical motion variables: w and $\dot{\eta}$. We therefore need an extra equation that naturally, but not necessarily [see Laprise (1992) for suggestions], comes from the kinematic equation:

$$\frac{dz}{dt} = w. \tag{16}$$

A complete transformation to the time-varying nonorthogonal curvilinear coordinate system considered here is of course possible but then the notions of four-dimensional tensor calculus become useful. It has been shown (Charron et al. 2013) that the present approach is mathematically equivalent. Counting the coordinate specification, $\eta = \eta(\mathbf{r}_h, z, t)$, the total number of equations and unknowns is brought to seven. Typically, η will be a nondimensional number ($0 \le \eta \le 1$). For example, $\eta = (z - z_S)/(z_T - z_S)$ with subscript S for bottom (Earth's surface) and T for top represents a terrain-following coordinate of the *height* type (Gal-Chen and Somerville 1975), while $\eta = p/p_S$ or $\eta = (p - p_T)/(p_S - p_T)$ (Phillips 1957), the so-called sigma coordinate, is of the *pressure* type. With an inverse relation of the form $p = A(\eta) + B(\eta)p_S$ (Simmons and Burridge 1981), we speak of the hybrid coordinate. For nonhydrostatic equations, a pressure-type coordinate is no longer suitable but may be replaced by one of the

TABLE 6. The four main discrete grid-equation configurations as selected from Table 3 and discussed in the text.

CP	R	L[a]	L[b]
—— w, b ——	—— w, b, u, P ——	—— w ——	—— w, P ——
– – u, P – –	– – – – – – – – – – – – – – – –	– – u, b, P – –	– – u, b – –
—— w, b ——	—— w, b, u, P ——	—— w ——	—— w, P ——
$i\nu u + ikP = 0$	$i\nu u + ikP = 0$	$i\nu u + ikP = 0$	$i\nu u + ik\overline{P}^z = 0$
$\delta_z w + iku = 0$	$\delta_z w + ik\overline{u}^z = 0$	$\delta_z w + iku = 0$	$\delta_z w + iku = 0$
$\delta_z P - b = 0$	$\delta_z P - \overline{b}^z = 0$	$\delta_z P - \overline{b}^z = 0$	$\delta_z P - b = 0$
$i\nu b + N_*^2 w = 0$	$i\nu b + N_*^2 w = 0$	$i\nu b + N_*^2 \overline{w}^z = 0$	$i\nu b + N_*^2 \overline{w}^z = 0$

hydrostatic-pressure type, $\pi = A(\eta) + B(\eta)\pi_S$ (Laprise 1992). Here, π is defined by the usual hydrostatic relation, $\partial\pi/\partial z = -g\rho$, or if we use (4) and introduce the geopotential, $\phi = gz$,

$$\frac{\partial\phi}{\partial\pi} = -\frac{RT}{p}. \tag{17}$$

This coordinate, with $\eta = \pi_*/p_T$ and π_* a number with pressure units varying between $p_{\rm ref} = 10^3$ hPa and p_T (the pressure at the model top), corresponds to that of GEM3 (Yeh et al. 2002). For GEM4 we instead write $\ln\pi = A(\zeta) + B(\zeta)s$, with $s = \ln(\pi_S/p_{\rm ref})$, ζ becoming a coordinate of the log-hydrostatic-pressure type and reserving the name η for the GEM3 coordinate. To allow for a clear distinction between GEM3 and GEM4, we may also define ζ as a coordinate transformation from η by the relation $\zeta = \zeta_S + \ln\eta$ where $\zeta_S = \ln(p_{\rm ref})$. This transformation is an invariant one, and η in (12)–(15) may simply be replaced by ζ. It is the introduction of ϕ and π through (17) that transforms (12)–(14) and (16), which we therefore rewrite as

$$\frac{d\mathbf{V}_h}{dt} + f\mathbf{k}\times\mathbf{V}_h + RT\nabla_\zeta \ln p + (1+\mu)\nabla_\zeta\phi = 0, \tag{18}$$

$$\frac{dw}{dt} - g\mu = 0, \tag{19}$$

$$\frac{d}{dt}\ln\left|\frac{\partial\pi}{\partial\zeta}\right| + \nabla_\zeta\cdot\mathbf{V}_h + \frac{\partial\dot\zeta}{\partial\zeta} = 0, \quad \text{and} \tag{20}$$

$$\frac{d\phi}{dt} - gw = 0, \tag{21}$$

introducing the nonhydrostatic index as

$$\mu = \frac{\partial p}{\partial\pi} - 1. \tag{22}$$

Returning to the coordinate definition, we adopt $A = \zeta$; hence, we write

$$\ln\pi = \zeta + Bs, \tag{23}$$

and for B, we use the following formula:

$$B = \left(\frac{\zeta-\zeta_T}{\zeta_S-\zeta_T}\right)^{r(\zeta)}, \tag{24}$$

with $\zeta_T = \ln\pi_T$ and where $r = r_{\max} - (r_{\max} - r_{\min})[(\zeta-\zeta_T)/(\zeta_S-\zeta_T)]$ is a variable exponent providing added freedom for adjusting the thickness of model layers over high terrain (Eckermann 2009). In Fig. 3, it is shown that judicious selection of $r_{\max}$ and $r_{\min}$ can minimize the problem of level compaction over high terrain while yielding quasi-horizontal coordinate surfaces in the stratosphere.

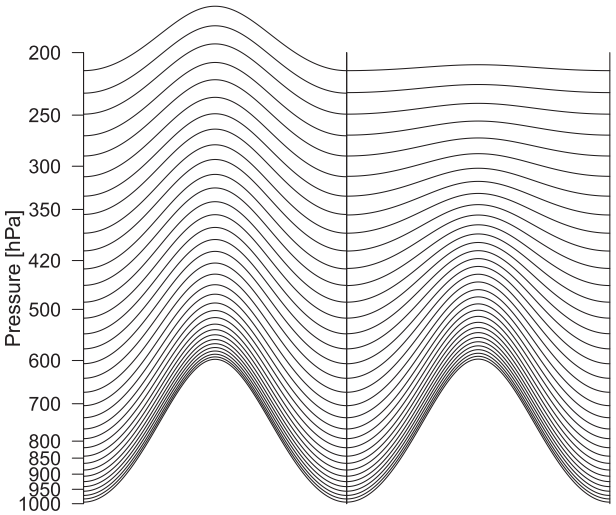

FIG. 3. Vertical model-level structure showing ζ levels as functions of pressure for values below 200 hPa (where the surface is at sea level) in a typical operational configuration. A sinusoidal mountain extending to 600 hPa in the center of the domain demonstrates the compaction of levels on high terrain. (left) The rectification coefficients are $r_{\min} = r_{\max} = 4.5$; (right) $r_{\min} = 2$ and $r_{\max} = 100$ provide a much faster rectification.

Finally, we summarize all the equations in terms of the basic model variables, the so-called history-carrying variables. We replace $\ln p$ by $\ln\pi + \ln(p/\pi) = \zeta + Bs + q$, eliminating π and introducing nonhydrostatic log-pressure deviation, $q = \ln(p/\pi)$. We replace ϕ by its deviation ($\phi' = \phi - \phi_*$) from $\phi_* = -RT_*(\zeta - \zeta_S)$, defining a basic-state temperature $T_* = \text{const}$ ($T_* = 240$ K is used with little sensitivity to this choice seen in practice). There are therefore six prognostic equations: the momentum [(18–19)], thermodynamic [(6)], continuity [(20)], and geopotential [(21)] which become

$$\frac{d\mathbf{V}_h}{dt} + f\mathbf{k}\mathrm{x}\mathbf{V}_h + RT\nabla_\zeta(Bs+q) + (1+\mu)\nabla_\zeta\phi' = 0, \tag{25}$$

$$\frac{dw}{dt} - g\mu = 0, \tag{26}$$

$$\frac{d}{dt}\left[\ln\left(\frac{T}{T_*}\right) - \kappa(Bs+q)\right] - \kappa\dot\zeta = 0, \tag{27}$$

$$\frac{d}{dt}\left[Bs + \ln\left(1+\frac{\partial B}{\partial\zeta}s\right)\right] + \nabla_\zeta\cdot\mathbf{V}_h + \frac{\partial\dot\zeta}{\partial\zeta} + \dot\zeta = 0, \quad \text{and} \tag{28}$$

$$\frac{d\phi'}{dt} - RT_*\dot\zeta - gw = 0. \tag{29}$$

We choose $\mathbf{V}_h, w, T, (\dot{\zeta}, s)$, and q as history-carrying variables. The two remaining unknowns, μ and ϕ', are obtained diagnostically from (22) and (17) and are rewritten as

$$1 + \mu - e^q \left[\frac{\partial q}{\partial(\zeta + Bs)} + 1 \right] = 0 \quad \text{and} \tag{30}$$

$$\frac{T}{T_*} + e^q \left[\frac{\partial(\phi'/RT_* + Bs)}{\partial(\zeta + Bs)} - 1 \right] = 0. \tag{31}$$

These are the GEM4 Euler equations to be discretized, in time as well as in space. A hydrostatic version is obtained if q is set to vanish for all times, in which case (26) and (30) are irrelevant while (29) is only pertinent if one wants to diagnose w. A particularity of the full equations is that they have characteristics of both height and hydrostatic-pressure coordinates. Gill (1982) named this type of coordinate z_* to emphasize its height character. Having $z_* = H_{\rm ref}(\zeta_S - \zeta)$, with $H_{\rm ref} = RT_{\rm ref}/g = 16\,000/\ln 10 \approx 6950$ m, would give a reasonable approximation to true heights. On the other hand, the continuity equation (28) has no reference to nonhydrostatic pressure and therefore remains characteristic of hydrostatic-pressure-type coordinates. One reason for using the log-hydrostatic-pressure coordinate ζ is the increased accuracy of the hydrostatic relation (31) aloft while resolution is degraded, a typical choice in NWP modeling. Logarithmic differencing of certain terms can of course be used independently of the coordinate definition. Another reason for our choice of coordinate is that the association of ζ with s and q, two model variables already of the logarithmic type, appears very natural and greatly simplifies the linearization of the equations to be undertaken in section 5.

There is of course arbitrariness in the choice of equations and variables. Here, we note the presence of logarithmic tendencies in (27) and (28), a fairly atypical feature. The presence of exponentials in the diagnostic equations (30) and (31) also attracts attention. In fact, just a slight change in the definition of hydrostatic pressure from (17) to $\partial\phi/\partial \ln\pi = -RT$ leads to their disappearance with the following result:

$$\mu - \frac{\partial q}{\partial(\zeta + Bs)} = 0 \quad \text{and}$$

$$\frac{T}{T_*} + \frac{\partial(\phi'/RT_* + Bs)}{\partial(\zeta + Bs)} - 1 = 0.$$

And, with apparently only a minor modification to the continuity equation (28),

$$\frac{d}{dt}\left[Bs + q + \ln\left(1 + \frac{\partial B}{\partial \zeta} s\right)\right] + \nabla_\zeta \cdot \mathbf{V}_h + \frac{\partial \dot{\zeta}}{\partial \zeta} + \dot{\zeta} = 0.$$

But the presence of nonhydrostatic pressure q in the continuity equation radically changes its character and we lose the advantages of the pressure-type coordinates without obtaining the advantages of the height-type coordinates. In particular, there appears to be a numerical instability characteristic of height-based models (see the appendix), as demonstrated by Bénard (2003) and Bénard et al. (2004). This is a sufficient reason for keeping (17).

4. Vertical discretization on the Charney–Phillips grid

The vertical discretization of (25)–(31) on the CP grid yields

$$\frac{d\mathbf{V}_h}{dt} + f\mathbf{k} \times \mathbf{V}_h + R\overline{T}^\zeta \nabla_\zeta (Bs + q) + (1 + \overline{\mu}^\zeta)\nabla_\zeta \phi' = 0, \tag{32}$$

$$\frac{dw}{dt} - g\mu = 0, \tag{33}$$

$$\frac{d}{dt}\left[\ln\left(\frac{T}{T_*}\right) - \kappa(\overline{B}^\zeta s + \overline{q}^\zeta)\right] - \kappa\dot{\zeta} = 0, \tag{34}$$

$$\frac{d}{dt}[Bs + \ln(1 + \delta_\zeta \overline{B}^\zeta s)] + \nabla_\zeta \cdot \mathbf{V}_h + \delta_\zeta \dot{\zeta} + \overline{\dot{\zeta}}^\zeta = 0, \tag{35}$$

$$\frac{d\overline{\phi'}^\zeta}{dt} - RT_* \dot{\zeta} - gw = 0, \tag{36}$$

$$1 + \mu - e^{\overline{q}^\zeta}\left[\frac{\delta_\zeta q}{\delta_\zeta(\zeta + Bs)} + 1 \right] = 0, \quad \text{and} \tag{37}$$

$$\frac{T}{T_*} + e^{\overline{q}^\zeta}\left[\frac{\delta_\zeta(\phi'/RT_* + Bs)}{\delta_\zeta(\zeta + Bs)} - 1 \right] = 0. \tag{38}$$

Vertical derivatives have been replaced by finite differences represented by the operator δ_ζ and averaging operators represented by overbars with superscript ζ (double averaging by an overbar with double superscripts) are introduced where required. Consistent with the CP-grid configuration described in section 2, $\mathbf{V}_h$, q, and ϕ' are defined on the same levels to be called full or ''momentum'' levels. They are staggered with respect to w, T, μ, and $\dot{\zeta}$, which are on ''half'' or ''thermodynamic'' levels. Note that the metric parameter B is defined on full levels and averaged rather than calculated on thermodynamic levels. In this discrete system, double operations

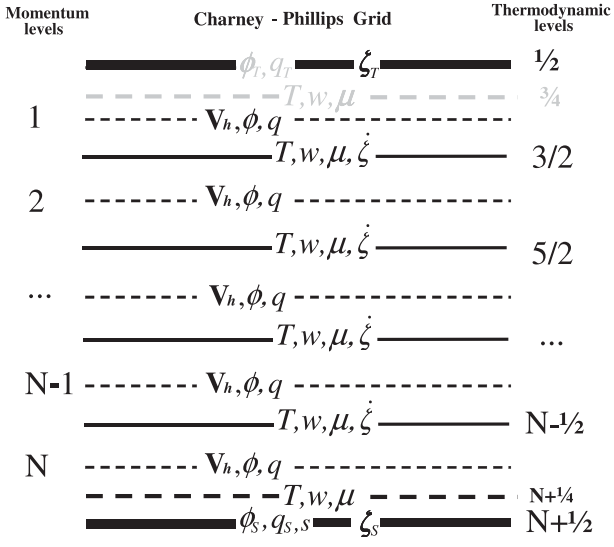

FIG. 4. The CP grid, giving the position occupied by each variable in the vertical domain. The model is composed of N layers, inside of which (in the middle of which only if the layers are equal) are the momentum levels $[1, 2, \ldots, N]$, where U, V, ϕ, and q are positioned but note that ϕ and q can also be defined on the boundaries. These N layers are delimited by $N - 1$ interfaces corresponding to the thermodynamic levels $[3/2, \ldots, N - 1/2]$, where T, w, μ, and $\dot{\zeta}$ are positioned, exactly in the middle of the momentum levels. For $\dot{\zeta}$, there are two additional levels [½ and $N + ½$] corresponding to the top and bottom surfaces. In addition, T, w, and μ have two additional levels [¾ and $N + 1/4$] positioned exactly in between, respectively, the top and first momentum level and the last momentum level and the surface. [The ¾ thermodynamic level and related variables (in gray) are absent from the *truncated top* (see end of section 5).]

on dependent variables are absent: no difference is calculated over more than two levels. The number of averaging operators is small: in the horizontal momentum equation (32), averaging is applied to nonlinear terms only; in the hydrostatic case (with $q = \mu = 0$ and w dropping out of the system), only one averaging operator remains on linear terms, namely on $\dot{\zeta}$ in the continuity equation (35). Note that averaging here could be replaced by weighted differencing since

$$\left(\frac{\partial}{\partial\zeta} + 1\right)\dot{\zeta} \equiv e^{-\zeta}\frac{\partial}{\partial\zeta}(e^{\zeta}\dot{\zeta}).$$

Taking into account the boundary conditions, $\dot{\zeta} = 0$, it is natural to have half levels coincide with the top and bottom. This describes the essence of the vertical grid shown in Fig. 4.

The placement of horizontal momentum, thermodynamic, continuity, and hydrostatic equations, as well as horizontal wind, temperature, geopotential, and vertical motion $\dot{\zeta}$, is the traditional one for hydrostatic models discretized on a CP grid (Daley et al. 1976). The placement of w on half levels is natural for nonhydrostatic models in height coordinates (Girard et al. 2005). Following these choices, the placement of the remaining equations and variables maximizing accuracy is straightforward. A puzzling aspect perhaps is the position of the geopotential tendency in equation (36) on half levels, resulting in an averaging operator on geopotential tendency itself. In section 5, we will form a numerical elliptic boundary value problem through variable elimination. We believe that the placement of equations and variables here adopted on the CP grid is in fact unique in allowing the elimination to proceed in harmony with the equivalent analytic process.

Some readers may wonder about the choices made near boundaries and appearing in Fig. 4. In particular, why the extra degrees of freedom for temperature afforded by ¼ and $N + 1/4$ thermodynamic levels? This has justly been argued against (Thuburn and Woollings 2005) and, perhaps, signals the return of problematic numerical modes. Models in height coordinates have been devised without such levels (Davies et al. 2005). The rationale for their retention in the present case is mostly based on the need for reliable near-surface and near-model-top temperatures in the assimilation component of the modeling system and the fact that such near-boundary levels are present in the previous model version, GEM3. The forecast model vertical resolution near the boundaries is still rather poor. In GEM4, the last momentum level corresponds to the second from last momentum level in GEM3 and sits at ~40 m above ground. Without the extra thermodynamic level, the last prognostic temperature would occur at approximately 80 m, clearly an unsatisfactory situation. Here, to allow for a fair comparison between the two model versions, we chose to adopt the strategy of making momentum levels coincide except at the surface. Thus, GEM4 ends up with the same number of staggered thermodynamic levels as GEM3 but with one fewer momentum level. Similar arguments do apply to the first thermodynamic level, as GEM4 cannot afford to lose this degree of freedom near the top when performing a strict comparison, but there are arguments in favor of its elimination, which are discussed in the next section.

As mentioned earlier, the finite differences replacing the derivatives are made as simple as possible. With ψ and χ standing for variables on full and half levels, respectively,

$$(\delta_{\zeta}\psi)_{k+1/2} = \frac{\psi_{k+1} - \psi_k}{\Delta\zeta_{k+1/2}} \qquad (k = 0, N) \quad \text{and}$$

$$\Delta\zeta_{k+1/2} = \zeta_{k+1} - \zeta_k$$

$$(\delta_\zeta \chi)_k = \frac{\chi_{k+1/2} - \chi_{k-1/2}}{\Delta\zeta_k} \qquad (k = 1, N),$$
$$\Delta\zeta_k = \zeta_{k+1/2} - \zeta_{k-1/2}$$

with the top, $\zeta_0 = \zeta_{1/2} = \zeta_T$; surface, $\zeta_{N+1} = \zeta_{N+1/2} = \zeta_S$; and momentum levels, $\zeta_k (1 \le k \le N)$; specified while intermediate thermodynamic levels, $\zeta_{k+1/2} = (\zeta_{k+1} + \zeta_k)/2$ $(1 \le k \le N-1)$, are calculated. For the two vertical means, we formally write

$$(\overline{\psi}^{\zeta})_{k+1/2} = \varpi^+_{k+1/2}\psi_{k+1} + \varpi^-_{k+1/2}\psi_k \qquad (k = 0, N)$$
$$\varpi^-_{k+1/2} = 1 - \varpi^+_{k+1/2}$$

and

$$(\overline{\chi}^{\zeta})_k = \varpi^+_k \chi_{k+1/2} + \varpi^-_k \chi_{k-1/2} \qquad (k = 1, N).$$
$$\varpi^-_k = 1 - \varpi^+_k$$

Averaging variables from full levels toward half levels follows the rule of calculation for half levels; that is,

$$\varpi^+_{1/2} = 0, \quad \varpi^+_{k+1/2} = \frac{1}{2} \quad (1 \le k \le N-1), \quad \varpi^+_{N+1/2} = 1.$$

This ensures optimal (second order) accuracy for the hydrostatic equation. Note the special values at both ends, however. To average variables from half levels toward full levels, three choices were considered: linear interpolation, simple average, and the averaging operator commuting with the difference operator. Due to a demonstrated lack of sensitivity, the latter was adopted mainly because it simplifies the algorithm as shown in the next section:

$$\varpi^+_k = \frac{\Delta\zeta_{k+1/2}}{2\Delta\zeta_k} \quad (1 \le k \le N-1),$$
$$\varpi^+_N = \frac{\Delta\zeta_{N+1/2}}{\Delta\zeta_N}. \tag{39}$$

5. The solution method

The horizontal and time discretizations are the same as in Côté et al. (1998) and Yeh et al. (2002). Parameterized forcings represented by **F** and Q in (1) and (2) remain added as a correction step (splitting method) and are thus not further considered here. For the purely dynamical step, an implicit iterative semi-Lagrangian scheme is used. Only the elements potentially affecting the vertical discretization will be dealt with in some detail here. The equation system can be summarized by

$$\frac{dF_i}{dt} + G_i = 0 \quad (i = h, w, \theta, C, \phi, \mu, H), \tag{40}$$

with index letters standing for the respective equations in the order that they appear in (32)–(38). One particularity of the present system is the fact that the F_i do not necessarily stand for history-carrying variables nor to a linear combination thereof. Also note that for the diagnostic relations, $F_i \equiv 0$ and therefore $G_i = 0$. Time discretization of (40) is written

$$\frac{F_i^A - F_i^D}{\Delta t} + bG_i^A + (1-b)G_i^D = 0, \tag{41}$$

where superscripts A and D, respectively, stand for "arrival" and "departure" space–time positions and where $b = \frac{1}{2} + \varepsilon_f$ with ε_f representing an off-centering parameter. For the diagnostic relations, we further have $G_i^A = 0$ and $G_i^D = 0$ independently. Separating arrivals and departures, we rewrite (41) as

$$\left(\frac{F_i}{\tau} + G_i\right)^A = \left(\frac{F_i}{\tau} - \beta G_i\right)^D \equiv R^D, \tag{42}$$

with $\tau = b\Delta t$ and $\beta = (1-b)/b$. To be solvable, the left-hand side of (42) is split into a linear part L^A and its nonlinear residual N^A:

$$L^A = \left(\frac{F_i}{\tau} + G_i\right)^A_{\text{lin}}; \tag{43}$$

Therefore,

$$N^A = \left(\frac{F_i}{\tau} + G_i\right)^A - \left(\frac{F_i}{\tau} + G_i\right)^A_{\text{lin}}. \tag{44}$$

The linearization procedure is standard and straightforward. The result (dropping the superscripts) of the linearization (43) of the system (32)–(38) is

$$\mathbf{L}_h = \frac{\mathbf{V}_h}{\tau} + \nabla_\zeta P,$$

$$L_w = \frac{w}{\tau} - g\mu,$$

$$L_\theta = \frac{T'}{\tau T_*} - \kappa X,$$

$$L_C = -\frac{1}{\tau}(\delta_\zeta \overline{q}^{\zeta} + \overline{q}^{\zeta\zeta}) + \nabla_\zeta \cdot \mathbf{V}_h + \delta_\zeta X + \overline{X}^{\zeta},$$

$$L_\phi = \frac{\overline{P}^{\zeta}}{\tau} - RT_* X - gw,$$

$$L_\mu = \mu - (\delta_\zeta q + \overline{q}^\zeta) \neq 0, \quad \text{and}$$

$$L_H = \frac{T'}{T_*} - (\delta_\zeta q + \overline{q}^\zeta) + \frac{\delta_\zeta P}{RT_*} \neq 0,$$

where $T' = T - T^*$ and after introducing the following temporary auxiliary variables

$$P \equiv \phi' + RT_*(Bs + q),$$

$$X \equiv \dot{\zeta} + \frac{\overline{B}^\zeta s + \overline{q}^\zeta}{\tau}.$$

For the rest of the discussion, we consider that the L_is are known quantities obtained by progressively improved estimates of the R_is and N_is:

$$L_i = R_i - N_i.$$

The solution process is iterative. The next step consists of combining the above linear system to form a single equation, having eliminated all variables except one. To achieve this, we first eliminate the diagnostic variables μ and T', combining the equations as shown:

$$L'_w \equiv L_w + gL_\mu = \frac{w}{\tau} - g(\delta_\zeta q + \overline{q}^\zeta),$$

$$L'_\theta \equiv L_\theta - \frac{L_H}{\tau} = \frac{1}{\tau}(\delta_\zeta q + \overline{q}^\zeta) - \frac{\delta_\zeta P}{\tau RT_*} - \kappa X.$$

Second, we eliminate $\mathbf{V}_h$ and q as follows:

$$L'_C \equiv \nabla_\zeta \cdot \mathbf{L}_h - \frac{1}{\tau}\left(L_C - \frac{\varepsilon}{w_*}\overline{L'^\zeta_w}\right) = \nabla^2_\zeta P - \frac{1}{\tau}(\delta_\zeta X + \overline{X}^\zeta) + \frac{\varepsilon \overline{w}^\zeta}{\tau^2 w_*},$$

$$L''_\theta \equiv \frac{\gamma}{\kappa\tau}\left(L'_\theta + \frac{\varepsilon}{w_*}L'_w + \frac{\varepsilon}{RT_*}L_\phi\right) = -\frac{\gamma}{\kappa\tau^2 RT_*}(\delta_\zeta P - \varepsilon\overline{P}^\zeta) - \frac{X}{\tau},$$

$$L'_\phi \equiv \frac{\gamma}{\kappa\tau}\left(L'_\theta + \frac{\varepsilon}{w_*}L'_w - \frac{\kappa}{RT_*}L_\phi\right) = -\frac{\gamma}{\kappa\tau^2 RT_*}(\delta_\zeta P + \kappa\overline{P}^\zeta) + \frac{w}{\tau^2 w_*},$$

where $w_* = RT_*/g\tau$, $\varepsilon = RT_*/g^2\tau^2$, and $\gamma = \kappa/(\kappa + \varepsilon)$. For the hydrostatic version, we simply need to set $\varepsilon = 0$. Commutation of the mean and difference operators assured by the weights (39) is such that $\delta_\zeta \overline{q}^\zeta = \overline{\delta_\zeta q}^\zeta$. Third, we eliminate w and X:

$$L''_C \equiv L'_C - (\delta_\zeta L''_\theta + \overline{L''_\theta}^\zeta) - \varepsilon\overline{L'^\zeta_\phi} = \nabla^2_\zeta P + \frac{\gamma}{\kappa\tau^2 RT_*}(\delta^2_\zeta P + \overline{\delta_\zeta P}^\zeta - \varepsilon(1-\kappa)\overline{P}^{\zeta\zeta}), \quad (45)$$

provided again that commutation holds and therefore $\delta_\zeta \overline{P}^\zeta = \overline{\delta_\zeta P}^\zeta$. In the vertical, this is a matrix inversion problem. For a model with N full levels, there are at this point $N + 2$ unknown values of P for N equations and N known values of L''_C, remembering that $L_i = R_i - N_i$. The extra equations required for solution are provided by L''_θ, applied at both the top and bottom (first and last thermodynamic levels). These become boundary conditions on P:

$$(L''_\theta)_T = -\frac{\gamma}{\kappa\tau^2 RT_*}(\delta_\zeta P - \varepsilon\overline{P}^\zeta)_T \quad \text{and} \quad (46)$$

$$(L''_\theta)_S = -\frac{\gamma}{\kappa\tau^2 RT_*}(\delta_\zeta P + \kappa\overline{P}^\zeta)_S + \frac{\phi_S}{\tau^2 RT_*}, \quad (47)$$

where $\dot{\zeta}_T = 0$, $B_T = 0$, and $q_T = 0$ at the top and $\dot{\zeta}_S = 0$ and $(Bs+q)_S = (P_S - \phi_S)/RT_*$ at the surface. This will be called the closed-top boundary condition. An open-top boundary condition has also been developed with this model formulation. We may combine L''_θ with L_θ as

$$\left(L''_\theta - \frac{L_\theta}{\kappa\tau}\right)_{\text{OpenT}} = -\frac{\gamma}{\kappa\tau^2 RT_*}(\delta_\zeta P - \varepsilon\overline{P}^\zeta)_{\text{OpenT}} - \frac{T'_{\text{OpenT}}}{\kappa\tau^2 T_*}, \quad (48)$$

thus eliminating X from the boundary conditions and having instead to specify the temperature (T'_{OpenT}) at the model top. We may then infer X_{OpenT} and therefore the inflow–outflow velocity $\dot{\zeta}_{\text{OpenT}}$. Of course, information must also be provided above the model top in order to satisfy the advection scheme. That this is a satisfactory open boundary condition in the hydrostatic case has been demonstrated (McTaggart-Cowan et al. 2011). In the nonhydrostatic case we also need to specify the nonhydrostatic pressure deviation, q_{OpenT}. Once the elliptic problem [(45) and (47), with (46) or (48)] is solved to find P, all the other variables are obtained by standard back substitution.

This discretized procedure of variable elimination leading to the elliptic equation precisely mimics the analytic procedure, replacing differences by derivatives and ignoring averages. In spite of this, given the nature

of the top boundary condition, the presence of temperature (Fig. 4) and the thermodynamic equation (34) at the top level is problematic. In effect, the equation is highly simplified due to the boundary condition: $d\ln T/dt = Q/c_pT$ since by construction $d\ln p/dt = 0$. Considering that vertical advection also vanishes, since $\dot{\zeta} = 0$, the resulting predicted temperature becomes poorly connected dynamically to the rest of the model. The ''disconnectedness'' is further amplified by the typical lack of vertical resolution of operational forecast models near the top. Finally, note that the closed-top boundary condition is itself very artificial. These factors seem to justify the elimination of the top thermodynamic equation and in fact the top thermodynamic level as a whole. A quick examination of the equations shows that, in the hydrostatic case, the top temperature only served to compute the pressure gradient term in the top horizontal momentum equation (32) and only if $B \neq 0$. At this level, B is small and can be made to vanish, in which case the top temperature is no longer required. Along with the top thermodynamic equation (34) and top temperature, the top hydrostatic equation (38) and top geopotential are no longer needed. In the nonhydrostatic case, the vertical momentum and geopotential equations [(33) and (36), respectively] may be eliminated provided we specify q (made to vanish) appearing in the top horizontal momentum equation (32). Thus, the elimination of all the equations and variables at the top thermodynamic level is complete with minimal arbitrariness. We have called this the truncated closed-top boundary condition.

6. Summary

This study was motivated by the fact that numerical noise detected in GEM3 was found to be in large part related to vertical discretization on a regular grid. While examining this issue of grid type within the context of vertically discretizing the Euler equations, we found that the R grid used by the GEM model was not only unpopular but also unfamiliar to the meteorological community. This despite the fact that its main properties, including accuracy, appeared comparable to those of the other main grids used: the Lorenz and Charney–Phillips grids. While comparing these grids, only one aspect seemed pertinent to the problem at hand, namely the presence or absence of stationary numerical modes as diagnosed from a simple eigenmode analysis. In this respect the R grid seemed to be unique in suffering from the presence of two such modes (the presence of one of them on the L grids being well known), both of which are absent from the CP grid. The elimination of such stationary numerical modes then seemed enough justification for modifying the dynamical core of GEM to discretize the equations on the CP grid.

Forecast models are known to concentrate their vertical resolution in the troposphere for obvious efficiency reasons and GEM is no exception. One known deficiency of GEM was its discretization of the hydrostatic equation using linear differencing. This, coupled with rapidly degrading resolution in the stratosphere, amounts to a loss of accuracy that can be at least partially alleviated by adopting logarithmic differencing where required. This prompted us to investigate a slightly different vertical coordinate of the log-hydrostatic-pressure type. Already the model's pressure-related variables, s and q, were logarithms of pressure ratios, a form that greatly simplifies the linearization process. Although well known to theorists, this is the first time such a coordinate is used in NWP as far as we know.

The discretization of the Euler equations transformed to log-hydrostatic-pressure coordinate using simple difference and average operators is a fairly straightforward process as shown, and the solution procedure using an implicit iterative semi-Lagrangian scheme is outlined. A distinguishing feature of the CP grid is the staggering of temperature and vertical motion with respect to horizontal motion. Assuming that vertical motion is defined at the boundaries (after all it vanishes in closed-top conditions and at the surface), this poses the problem of what to do with the temperature. For the open-top condition, carrying temperature on the boundary was shown to be useful by McTaggart-Cowan et al. (2011). We believe the issue of carrying temperature on, or near to, closed boundaries for NWP applications is still not well resolved. We have argued against such a level near the top, suggesting a truncated closed-top boundary condition, and in favor of maintaining one near the surface when vertical resolution is rather poor.

The GEM4 model described here has been operational in most of the forecasting applications at the CMC since 2012. In a follow-up study, we plan to discuss the implementation problems encountered, in particular issues involving the adaptation of the semi-Lagrangian advection scheme and physical parameterization schemes to a staggered vertical grid. The GEM3 and GEM4 models will be compared in a controlled situation involving actual forecasts as well as idealized model integrations. The impacts of the changes will be presented, demonstrating that the Euler equations as formulated and discretized in GEM4 indeed lead to improved model stability (reduction of noise) and accuracy, and ultimately to improved operational forecasts.

Acknowledgments. The authors wish to thank Celal Konor and an anonymous reviewer for their careful reviews of this paper.

APPENDIX

Stability and the Definition of Hydrostatic Pressure

As mentioned at the end of section 3, defining hydrostatic pressure (π) unconventionally, as $\partial\phi/\partial \ln\pi = -RT$, changes the character of the continuity equation and leads to a numerical instability typical of height-based models. Here, we show how this instability arises, closely following the procedure established by Bénard et al. (2004). With the nonconventional definition of π, the linear system takes the form

$$\begin{aligned}
\partial_t \mathbf{V}_h + R\overline{T}\nabla_\zeta(Bs+q) + \nabla_\zeta \phi'' &= 0,\\
\partial_t w - g\partial_\zeta q &= 0,\\
\partial_t[T'' - \kappa\overline{T}(Bs+q)] - \kappa\overline{T}\dot{\zeta} &= 0,\\
\partial_t[(Bs+q) + s\partial_\zeta B] + \nabla_\zeta \cdot \mathbf{V}_h + \dot{\zeta} + \partial_\zeta\dot{\zeta} &= 0,\\
\partial_t\phi'' - R\overline{T}\dot{\zeta} - gw &= 0,\\
RT'' + \partial_\zeta\phi'' &= 0,
\end{aligned}$$

with the notation $\partial_t \equiv \partial/\partial t, \partial_\zeta \equiv \partial/\partial\zeta$. Here, $\overline{T}$ is the mean, $T'' = T - \overline{T}$, and ϕ'' is computed accordingly. The acoustic linear system (vertical only) is then

$$\begin{aligned}
\partial_t w - g\partial_\zeta q &= 0,\\
\partial_t(T'' - \kappa\overline{T}q) - \kappa\overline{T}\dot{\zeta} &= 0,\\
\partial_t q + \dot{\zeta} + \partial_\zeta\dot{\zeta} &= 0,\\
\partial_t\phi'' - R\overline{T}\dot{\zeta} - gw &= 0,\\
RT'' + \partial_\zeta\phi'' &= 0.
\end{aligned}$$

Assuming solutions of the form $f \sim e^{n\zeta - i\omega t}$ leads to the *dispersion relation*:

$$\omega^2 = -\frac{g^2 n(1+n)}{(1-\kappa)R\overline{T}} = \frac{g^2\left(\nu^2 + \frac{1}{4}\right)}{(1-\kappa)R\overline{T}},$$

where ω is real when $n = i\nu - 1/2$. Consider now the following *time discretization* [using simple difference (δ_t) and average operators (overbars with index t) essentially corresponding to the first iteration of the model's implicit scheme] with $T' = T - T_*$:

$$\begin{aligned}
\delta_t w - g\partial_\zeta \overline{q}^t &= 0,\\
\delta_t[T' - \kappa\overline{T}q] - \kappa T_*(\overline{\dot{\zeta}}^t + \alpha\dot{\zeta}) &= 0,\\
\delta_t q + \overline{\dot{\zeta} + \partial_\zeta\dot{\zeta}}^t &= 0,\\
\delta_t\phi' - RT_*\overline{\dot{\zeta}}^t - g\overline{w}^t &= 0,\\
RT' + \partial_\zeta\phi' &= 0,
\end{aligned}$$

where $\alpha = \overline{T}/T_* - 1$. Going back to the true perturbation variables, T'' and ϕ'', where $T'' = T' - \alpha T_*$ and $\phi'' = \phi' + \alpha RT_*\zeta + \text{const}$, we have that $\delta_t T' = \delta_t T''$ and $\delta_t\phi' = \delta_t\phi'' - \alpha RT_*\dot{\zeta}$. Thus,

$$\begin{aligned}
\delta_t w - g\partial_\zeta \overline{q}^t &= 0,\\
\delta_t[T'' - \kappa\overline{T}q] - \kappa T_*(\overline{\dot{\zeta}}^t + \alpha\dot{\zeta}) &= 0,\\
\delta_t q + \overline{\dot{\zeta} + \partial_\zeta\dot{\zeta}}^t &= 0,\\
\delta_t\phi'' - RT_*(\overline{\dot{\zeta}}^t + \alpha\dot{\zeta}) - g\overline{w}^t &= 0,\\
RT'' + \partial_\zeta\phi'' &= 0,
\end{aligned}$$

leading to the *discrete dispersion relation*:

$$\frac{\tan^2(\omega\Delta t/2)}{(\Delta t/2)^2}\left[1 + \frac{i\tan(\omega\Delta t/2)\alpha}{(1-\kappa)(1+\alpha)}\left(1 + \frac{\kappa}{n}\right)\right] = \frac{g^2\left(\nu^2 + \frac{1}{4}\right)}{(1-\kappa)R\overline{T}}.$$

The absence of averaging on certain terms (the α terms) allows solutions to become complex. Therefore, this nonhydrostatic version of the model is unstable. The problem is due to the presence of the term $\delta_t q$ in the continuity equation, which arises from the definition of π.

Conversely, with the traditional definition of hydrostatic pressure ($\partial\phi/\partial\pi = -RT/p$), the linear acoustic system becomes analytically

$$\begin{aligned}
\partial_t w - g(q + \partial_\zeta q) &= 0,\\
\partial_t(T'' - \kappa\overline{T}q) - \kappa\overline{T}\dot{\zeta} &= 0,\\
\dot{\zeta} + \partial_\zeta\dot{\zeta} &= 0,\\
\partial_t\phi'' - R\overline{T}\dot{\zeta} - gw &= 0,\\
RT'' - R\overline{T}q + \partial_\zeta\phi'' &= 0,
\end{aligned}$$

and numerically

$$\begin{aligned}
\delta_t w - g\overline{(\partial_\zeta q + q)}^t &= 0,\\
\delta_t(T'' - \kappa\overline{T}q) - \kappa T_*(\overline{\dot{\zeta}}^t + \alpha\dot{\zeta}) &= 0,\\
\overline{\dot{\zeta} + \partial_\zeta\dot{\zeta}}^t &= 0,\\
\delta_t\phi'' - RT_*(\overline{\dot{\zeta}}^t + \alpha\dot{\zeta}) - g\overline{w}^t &= 0,\\
RT'' - R\overline{T}q + \partial_\zeta\phi'' &= 0.
\end{aligned}$$

Here, $\dot{\zeta} = 0$ is a solution independent of the rest of the system and the dispersion relation becomes

$$\frac{\tan^2(\omega\Delta t/2)}{(\Delta t/2)^2} = \frac{g^2\left(\nu^2 + \frac{1}{4}\right)}{(1-\kappa)R\overline{T}},$$

with ω always real. The integration step is therefore stable.

REFERENCES

Arakawa, A., 1988: Finite-difference methods in climate modeling. *Physically-Based Modeling and Simulation of Climate and Climate Change,* Vol. I, M. Schlesinger, Ed., D. Reidel, 79–168.

——, and S. Moorthi, 1988: Baroclinic instability in vertically discrete systems. *J. Atmos. Sci.,* **45,** 1688–1707.

——, and C. S. Konor, 1996: Vertical differencing of the primitive equations based on the Charney–Phillips grid in hybrid σ–p vertical coordinates. *Mon. Wea. Rev.,* **124,** 511–528.

Bénard, P., 2003: Stability of semi-implicit and iterative centered-implicit time discretizations for various equation systems used in NWP. *Mon. Wea. Rev.,* **131,** 2479–2491.

——, R. Laprise, J. Vivoda, and P. Smolikova, 2004: Stability of leapfrog constant-coefficients semi-implicit schemes for the fully elastic system of Euler equations: Flat-terrain case. *Mon. Wea. Rev.,* **132,** 1306–1318.

Charney, J. C., and N. A. Phillips, 1953: Numerical integration of the quasi-geostrophic equations for barotropic and simple baroclinic flows. *J. Meteor.,* **10,** 17–29.

Charron, M., A. Zadra, and C. Girard, 2013: Four-dimensional tensor equations for a classical fluid in an arbitrary gravitational field. *Quart. J. Roy. Meteor. Soc.,* doi:10.1002/qj.2185, in press.

Côté, J., S. Gravel, A. Méthot, A. Patoine, M. Roch, and A. Staniforth, 1998: The operational CMC–MRB Global Environmental Multiscale (GEM) model. Part I: Design considerations and formulation. *Mon. Wea. Rev.,* **126,** 1373–1395.

Daley, R., C. Girard, J. Henderson, and I. Simmonds, 1976: Short-term forecasting with a multi-level spectral primitive equation model. Part I—Model formulation. *Atmosphere,* **14,** 98–116.

Davies, T., M. J. P. Cullen, A. J. Malcolm, M. H. Mawson, A. Staniforth, A. A. White, and N. Wood, 2005: A new dynamical core for the Met Office's global and regional modeling of the atmosphere. *Quart. J. Roy. Meteor. Soc.,* **131,** 1759–1782.

Eckermann, S., 2009: Hybrid σ–p coordinate choices for a global model. *Mon. Wea. Rev.,* **137,** 224–245.

Fox-Rabinovitz, M. S., 1994: Computational dispersion properties for vertically staggered grids for atmospheric models. *Mon. Wea. Rev.,* **122,** 377–392.

Gal-Chen, T., and R. C. Somerville, 1975: On the use of a coordinate transformation for the solution of Navier–Stokes equations. *J. Comput. Phys.,* **17,** 209–228.

Gill, A. E., 1982: *Atmosphere–Ocean Dynamics.* Academic Press, 662 pp.

Girard, C., R. Benoît, and M. Desgagné, 2005: Finescale topography and the MC2 dynamics kernel. *Mon. Wea. Rev.,* **133,** 1463–1477.

Hollingsworth, A., 1995: A spurious mode in the ''Lorenz'' arrangement of ϕ and T which does not exist in the ''Charney–Phillips'' arrangement. ECMWF Tech. Memo. 211, 12 pp.

Kasahara, A., 1974: Various vertical coordinate systems used for numerical weather prediction. *Mon. Wea. Rev.,* **102,** 509–522.

Laprise, R., 1992: The Euler equations of motion with hydrostatic pressure as independent variable. *Mon. Wea. Rev.,* **120,** 192–207.

——, and C. Girard, 1990: A spectral general circulation model using piecewise-constant finite-element representation on a hybrid vertical coordinate system. *J. Climate,* **3,** 32–52.

Lorenz, E. N., 1960: Energy and numerical weather prediction. *Tellus,* **12,** 364–373.

McTaggart-Cowan, R., C. Girard, A. Plante, and M. Desgagné, 2011: The utility of upper-boundary nesting in NWP. *Mon. Wea. Rev.,* **139,** 2117–2144.

Phillips, N. A., 1957: A coordinate system having some special advantages for numerical forecasting. *J. Meteor.,* **14,** 184–185.

——, 1966: The equations of motion for a shallow rotating atmosphere and the ''traditional approximation.'' *J. Atmos. Sci.,* **23,** 626–628.

Qaddouri, A., and V. Lee, 2011: The Canadian Global Environmental Multiscale model on the Yin–Yang grid system. *Quart. J. Roy. Meteor. Soc.,* **137,** 1913–1926.

Ritchie, H., 1991: Application of the semi-Lagrangian method to a multilevel spectral primitive-equations model. *Quart. J. Roy. Meteor. Soc.,* **117,** 91–106.

Robert, A., J. Henderson, and C. Turnbull, 1972: An implicit time integration scheme for baroclinic models of the atmosphere. *Mon. Wea. Rev.,* **100,** 329–335.

Simmons, A. J., and D. M. Burridge, 1981: An energy and angular-momentum conserving vertical finite-difference scheme and hybrid vertical coordinates. *Mon. Wea. Rev.,* **109,** 758–766.

Tanguay, M., A. Simard, and A. Staniforth, 1989: A three-dimensional semi-Lagrangian scheme for the Canadian regional finite-element forecast model. *Mon. Wea. Rev.,* **117,** 1861–1871.

——, A. Robert, and R. Laprise, 1990: A semi-implicit semi-Lagrangian fully compressible regional forecast model. *Mon. Wea. Rev.,* **118,** 1970–1980.

Thomas, S. J., C. Girard, R. Benoit, M. Desgagné, and P. Pellerin, 1998: A new adiabatic kernel for the MC2 model. *Atmos.–Ocean,* **36,** 241–270.

Thuburn, J., and T. J. Woollings, 2005: Vertical discretizations for compressible Euler equation atmospheric models giving optimal representation of normal modes. *J. Comput. Phys.,* **203,** 386–404.

Tokioka, T., 1978: Some considerations on vertical differencing. *J. Meteor. Soc. Japan,* **56,** 98–111.

Yakimiw, E., and C. Girard, 1987: Experimental results on the accuracy of a global forecast spectral model with different vertical discretization schemes. *Atmos.–Ocean,* **25,** 304–325.

Yeh, K.-S., J. Côté, S. Gravel, A. Méthot, A. Patoine, M. Roch, and A. Staniforth, 2002: The CMC–MRB Global Environmental Multiscale (GEM) model. Part III: Nonhydrostatic formulation. *Mon. Wea. Rev.,* **130,** 339–356.

Zadra, A., M. Buehner, S. Laroche, and J.-F. Mahfouf, 2004: Impact of the GEM model simplified physics on extratropical singular vectors. *Quart. J. Roy. Meteor. Soc.,* **130,** 2541–2569.